bioRxiv preprint doi: https://doi.org/10.1101/003863; this version posted April 8, 2014. The copyright holder for this preprint (which was not certified by peer review) is the author/funder, who has granted bioRxiv a license to display the preprint in perpetuity. It is made available under aCC-BY-ND 4.0 International license.

The micron-scale structural organization of hippocampal area CA1 neuropil

Author: Yuriy Mishchenko

Affiliation: Toros University, Mersin, Turkey

Address: Toros University, 45 Evler Campus, Yenisehir 33140, Mersin, Turkey

Contact: yuriy.mishchenko@gmail.com, 90 324 325 33 00

Running title: Micron-scale organization of hippocampal area CA1 neuropil

bioRxiv preprint doi: https://doi.org/10.1101/003863; this version posted April 8, 2014. The copyright holder for this preprint (which was not certified by peer review) is the author/funder, who has granted bioRxiv a license to display the preprint in perpetuity. It is made available under aCC-BY-ND 4.0 International license.

ABSTRACT

Various structures in the brain contain many important clues to the brain's development and function. Among these, the organization of neuropil tissue at micron scales is of particular importance since such organization has a direct potential to affect the formation of synaptic connectivity between nearby axons and dendrites, thus, serving as an important factor contributing to the brain's development and disorders. While the organization of the brain at large and intermediate scales had been well studied, the microscopic organization of neuropil tissue remains largely unknown. In particular, presently it is not known what specific structures exist in neuropil at micron scales, what effect such structures have on synaptic connectivity, and what processes shape the neuropil's organization at micron scales. The present work performs an analysis of recent complete electron microscopy reconstructions of blocks of hippocampal CA1 neuropil tissue in rat to produce answers to these questions. We use a novel statistical approach to analyze the small-scale organization of neuropil systematically and to show that such organization can be well understood in terms of disordered, random arrangement of axonal and dendritic processes without significant local order. We also discuss several deviations from this simple picture observed in the distributions of glia and dendritic spines. Finally, we examine the question of the relationships between local neuropil's organization and synaptic connectivity.

KEYWORDS: neural tissue organization, neuropil organization, neuroanatomy, electron microscopy reconstruction, neurodegeneration, radial distribution function,

bioRxiv preprint doi: https://doi.org/10.1101/003863; this version posted April 8, 2014. The copyright holder for this preprint (which was not certified by peer review) is the author/funder, who has granted bioRxiv a license to display the preprint in perpetuity. It is made available under aCC-BY-ND 4.0 International license.

INTRODUCTION

Understanding the brain's anatomical structure is an important goal of neuroscience both from the point of view of producing new insights into the principles of brain's organization (Arbib et al., 1997; Bono and Villu Maricq, 2005; Hatton, 1990; Sporns et al., 2004, 2005) and better understanding of the brain's development and disorders (Brambilla et al., 2003; Castellanos et al., 2002; Garrard et al., 1998; Geschwind, 1975; Good et al., 2002; Uhlhaas and Singer, 2006). Diverse anatomical structures are readily observable in the brain at a variety of scales. At the largest scale, the organization of the brain into specific regions and functional areas has been well established (Brodmann and Garey, 2005; Damasio, 2005; Kandel et al., 2000). At intermediate scales, the structures such as cortical layers (Kandel et al., 2000; Nolte, 2002), cortical columns (Freeman, 2003), topographic mappings (Adams and Horton, 2003; Montero et al., 1977), ocular dominance patterns (Erwin et al., 1995; Miller et al., 1989), and orientation selectivity patterns (Bosking et al., 1997; Ohki et al., 2005) are also apparent. A range of genetic, biomolecular, and neural activity mechanisms are known to be associated with the formation and development of these structures, serving as important clues about the brain's development and disorders (Dickson, 2002; Ferster and Miller, 2000; Keil et al., 2010; McLaughlin and O'Leary, 2005; Parrish et al., 2007; Tear, 1999; Wolf et al., 2011; Wong, 1999).

Despite this extensive body of knowledge, the micron-scale organization of neural tissue in the brain remains essentially unknown. Such organization is of particular importance since it can directly affect the formation of synaptic connectivity between nearby axons and dendrites, thus, serving as potentially important factor contributing to neurodegenerative disorders, which are frequently characterized by degeneration of synaptic connectivity in neural tissues (Bonda et al., 2010; Hamos et al., 1989; Raff et al., 2002; Scheff et al., 2006; Terry, 2000). Although a number of past anatomical studies had examined microscopic structures in neural tissues (Braitenberg and Schuz, 1998; Chicurel and Harris, 1992; Fiala and Harris, 2001; Shepherd and Harris, 1998), the organization of the neural tissue itself as well as its interplay with neuronal connectivity remained largely beyond the scope of such studies. In particular, presently we do not know what specific structures exist in neuropil at micron scales, how such structures affect synaptic connectivity, and what neurobiological factors are responsible for shaping the structural organization of neuropil at micron scales.

In the present study, we intend to produce insights into these questions by analyzing recent serial section Transmission Electron Microscopy (ssTEM) reconstructions of contiguous volumes of rat hippocampal CA1 neuropil at nanometer scale (Mishchenko,

bioRxiv preprint doi: https://doi.org/10.1101/003863; this version posted April 8, 2014. The copyright holder for this preprint (which was not certified by peer review) is the author/funder, who has granted bioRxiv a license to display the preprint in perpetuity. It is made available under aCC-BY-ND 4.0 International license.

2009; Mishchenko et al., 2010). We use a novel systematic approach for such analysis, based on the statistical tool of radial distribution functions (Chandler, 1987; McQuarrie, 2000; Sandler, 2010). Radial distribution functions are commonly employed in statistical physics to characterize the organization of complex materials such as alloys, solutions, and colloids. Radial distribution functions are measured as the density of particles of different sorts at different distances away from a selected reference particle in material, and characterize the spatial correlations present among the material's different structural components. For example, in ordered materials such as solutions or colloids the radial distribution functions are known to exhibit pronounced peaks and features indicative of spatial correlations existing in such materials, while the radial distribution functions in disordered materials such as gases are typically featureless, indicating lack of any correlations (Chandler, 1987; McQuarrie, 2000; Sandler, 2010) . (See also Suppl. Figure A for additional details.)

We suitably modify the definition of radial distribution functions to be applicable in the case of micron-scale neural tissue, and use it to measure directly the radial distribution functions in hippocampal neuropil reconstructions in (Mishchenko, 2009; Mishchenko et al., 2010). We perform a detailed analysis of thus produced measurements using statistical and modeling approaches, and demonstrate that the organization of hippocampal neuropil tissue at micron scales is disordered or stochastic. We also discuss deviations from stochastic organization in the micron-scale distributions of glia and dendritic spines in neuropil. Finally, we inspect the variations in different dendritic segments' dendritic spine densities in the sample in relation to the organization of the surrounding neuropil, and show that no significant correlations exist between these two variables. This indicates that synaptic connectivity in hippocampal neuropil tissue is not affected by the organization of immediately surrounding neuropil (Mishchenko et al., 2010).

MATERIALS AND METHODS

Reconstructions of hippocampal area CA1 neuropil. Four approximately cubic volumes of hippocampal CA1 neuropil, totaling close to 670 μm^3 and 1900 neural processes fragments, were reconstructed using ssTEM in (Mishchenko et al., 2010). Volumes 1, 3, and 4 of these, in the nomenclature of (Mishchenko et al., 2010), were used to carry out the analysis in this work. The volume 2 was not used because of its small size – this volume comprised 30 μm^3 block of neuropil around a single dendritic spine. All volumes were from the middle of s. radiatum about 150 to 200 microns from the hippocampal CA1 pyramidal cell soma. Volumes 1 and 3 were from hippocampal area CA1 of a perfusion-fixed male rat of the Long-Evans strain weighing 310 gm

bioRxiv preprint doi: https://doi.org/10.1101/003863; this version posted April 8, 2014. The copyright holder for this preprint (which was not certified by peer review) is the author/funder, who has granted bioRxiv a license to display the preprint in perpetuity. It is made available under aCC-BY-ND 4.0 International license.

(postnatal day 77, (Harris and Stevens, 1989)), and volume 4 was from a hippocampal slice from a postnatal day 21 male rat of the Long-Evans strain as described in (Fiala et al., 2003). In order to perform the reconstructions, the series of ultrathin sections were cut from these volumes at ~45-50 nm using a ultramicrotome, mounted and counter stained with saturated ethanolic uranyl acetate followed by Reynolds lead citrate, and photographed on JEOL 1200EX and 1230 electron microscope (JEOL, Peabody, MA) at 10,000X or 5,000X. The contents of these volumes was subsequently reconstructed from the stacks of produced micrograph images at resolution 4.4 nm/pixel using the automated approach of (Mishchenko, 2009).

Measurement of radial distribution functions. In order to calculate the radial distribution functions for axonal, dendritic, spine, and glia components in hippocampal neuropil, we first constructed a series of equidistant radial surfaces outwards from the surface of each of approximately 1500 neural processes in the reconstructed neuropil samples. This was done in Matlab using fast anisotropic 3D distance transform function "bwdistsc" (Mishchenko, 2013). The radial shells were defined so as to correspond to the space between two consecutive equidistant surfaces at step of 13.2 nm in volumes 1 and 3 and 8 nm in volume 4. The difference was due to different pixel size in volume 4, that is, 8 nm/pixel. Subsequently, in order to calculate the radial distribution functions, for each radial shell and each neural process the average density of different neuropil components was calculated, and then averaged over all axons and dendrites to produce class-specific average radial distribution functions. In the case of dendrites, additionally an automatic morphological spine truncation algorithm was applied prior to calculating radial distributions to remove spines from dendritic shafts at the base of narrow spine-necks, in order to measure the radial distributions only relative to the dendritic shafts. Each dendritic shafts was also manually verified, to confirm that each shaft was obtained by the algorithm correctly.

Measurement of the size distributions of axonal and dendritic cross-sections. In order to measure the distribution of the local sizes of axonal and dendritic cross-sections in hippocampal neuropil, we first evaluate the 3D distance transform inwards of each neural process in the samples. This calculation was performed in Matlab using the fast anisotropic 3D distance transform function "bwdistsc" (Mishchenko, 2013). In this way, for each pixel in reconstructed volumes the value of the shortest distance from that pixel to the containing neural process's surface was calculated. The centerline of each neural process was subsequently defined as the set of points where such distance transform had a local maximum in at least two out of three orthogonal directions. The distance values along the centerlines were then collected for each neural process, in order to provide the characterization of the size distribution of the diameters of its cross-sections at a step of

bioRxiv preprint doi: https://doi.org/10.1101/003863; this version posted April 8, 2014. The copyright holder for this preprint (which was not certified by peer review) is the author/funder, who has granted bioRxiv a license to display the preprint in perpetuity. It is made available under aCC-BY-ND 4.0 International license.

approximately 50 nm. The class-averages were then computed over all axonal, dendritic, and spine-head objects.

The model of random mixing of local neuropil. To quantitatively describe the salient features of the measured neuropil radial distribution functions (Figure 2), we develop here a model of random mixing of local neuropil. We consider the process of moving a thin radial shell away from the surface of one reference axon or dendrite, while keeping track of the average density of other axonal and dendritic processes inside such shell. Two processes should be considered during such motion: i) some of the axons and dendrites earlier present in the shell terminate, and ii) new dendrites and axons appear in thus vacated spaces. If the average diameters of axonal and dendritic processes can be described by d_{axn} and d_{dnd}, the probability of an axon or a dendrite terminating inside the radial shell as it moves over distance Δx can be approximately described as $\Delta x/d_{axn}$ and $\Delta x/d_{dnd}$, respectively. Subsequently, vacated space should be re-partitioned among newly emerging axons and dendrites. In random mixing model, such re-partitioning occurs randomly in the ratio of the surface areas of newly emerged axons and dendrites, which can be approximately described by the global ratio of the surface areas of axonal and dendritic processes in the sample, $n_{axn}\pi d_{axn}L : n_{dnd}\pi d_{dnd}L$. Here, L is the linear size of the sample volume and πdL is the surface area of one neural process viewed as a cylinder of diameter d and length L, and n_{axn} and n_{dnd} are the number densities of axons and dendrites in the volume.

If we denote the relative density of axonal and dendritic processes in the radial shell at distance x away from the reference axon or dendrite as $N_{axn}(x)$ and $N_{dnd}(x)$, respectively, the above two processes can be mathematically represented as two equations for the evolution of $N_{axn}(x)$ and $N_{dnd}(x)$ with x;

$$\Delta N_{axn}(x) = -N_{axn}(x)\frac{\Delta x}{d_{axn}} + \frac{n_{axn}d_{axn}}{n_{axn}d_{axn} + n_{dnd}d_{dnd}}\left(N_{axn}(x)\frac{\Delta x}{d_{axn}} + N_{dnd}(x)\frac{\Delta x}{d_{dnd}}\right)$$

$$\Delta N_{dnd}(x) = -N_{dnd}(x)\frac{\Delta x}{d_{dnd}} + \frac{n_{dnd}d_{dnd}}{n_{axn}d_{axn} + n_{dnd}d_{dnd}}\left(N_{axn}(x)\frac{\Delta x}{d_{axn}} + N_{dnd}(x)\frac{\Delta x}{d_{dnd}}\right)$$

The first term in these equations represents the termination of axons and dendrites in the radial shell with frequency $\Delta x/d_{axn}$ and $\Delta x/d_{dnd}$, and the second term represents the random re-partitioning of the vacated space among newly emerging axons and dendrites in the ratio of axonal and dendritic surface areas $n_{axn}d_{axn}$ and $n_{dnd}d_{dnd}$. Note that $N(x)$ are relative densities, that is, $N_{axn}(x) + N_{dnd}(x) = 1$ at all times.

The above evolution equations can be solved using standard methods and these solutions yield several immediate predictions. Specifically, at small distances, $x \approx 0$, the radial

bioRxiv preprint doi: https://doi.org/10.1101/003863; this version posted April 8, 2014. The copyright holder for this preprint (which was not certified by peer review) is the author/funder, who has granted bioRxiv a license to display the preprint in perpetuity. It is made available under aCC-BY-ND 4.0 International license.

distribution functions are found to have the ratio equal to that of the total surface areas of dendritic and axonal processes, $N_{axn}(x \approx 0): N_{dnd}(x \approx 0) \approx n_{axn} d_{axn} : n_{dnd} d_{dnd}$, which can be seen by taking $N_{axn}(0) = 1$ or $N_{dnd}(x) = 1$ and performing a single step Δx. At large distances, the asymptotic values of the neuropil structure functions are defined by the average volume densities of axonal and dendritic processes, $N_{axn}(\infty): N_{dnd}(\infty) \approx n_{axn} {d_{axn}}^2 : n_{dnd} {d_{dnd}}^2$, which can be seen by considering $\Delta N_{axn}(x) = \Delta N_{dnd}(x) = 0$. Given $d_{dnd} > d_{axn}$, these ratios should differ by the factor of $d_{dnd}/d_{axn} \approx 3.3$ (Table 3 in (Mishchenko et al., 2010)). The transition between the small distance and large distance regimes occurs exponentially on the scale $l \approx d_{dnd} \frac{1+S_{dnd}/S_{axn}}{1+V_{dnd}/V_{axn}} \approx 500$ nm, where $S_{dnd}/S_{axn} \approx 1/6$ and $V_{dnd}/V_{axn} \approx 1/2$ are the ratios of dendritic and axonal surface and volume fractions in the samples, respectively (Figure 2 in (Mishchenko et al., 2010)). Finally, the radial distribution functions are the same whether the initial reference object was chosen as an axon or a dendrite, that is, the dendritic and axonal structure functions should not differ. Direct inspection of Figure 2 in Results demonstrates that all of these predictions are in excellent agreement with the direct measurements of the radial distribution functions in neuropil.

RESULTS

1. Organization of hippocampal CA1 neuropil at micron scales

Recently, dense reconstruction of complete volumes of neuropil tissue had been produced using electron microscopy, Figure 1. A quick inspection of these reconstructions reveals complex small-scale organization of neuropil without apparent patterns. Still, one cannot immediately conclude whether apparent lack of features in neuropil's small-scale organization is due to the absence of any structure in neuropil at micron-scale or because such structure is complex and visually obscured. In order to provide an answer to this question, we use here in the context of the small-scale structural organization of neuropil the statistical approach of radial distribution functions (Chandler, 1987; McQuarrie, 2000; Sandler, 2010).

Radial distribution functions at given distance *r* are defined conventionally as the average density of particles of different sorts in a radial shell distance *r* away from a selected reference particle in material. In the case of neuropil, we define the radial distribution functions as the average density of neural processes of different kinds, such as axons, dendrites, spines or glia, at different distances away from the surface of a given reference neural process, see Figure 2A. This modified definition has to be used because of the fiber-like and irregular shapes of axonal and dendritic processes predominantly comprising neuropil. The radial distribution functions defined in this way quantify the

bioRxiv preprint doi: https://doi.org/10.1101/003863; this version posted April 8, 2014. The copyright holder for this preprint (which was not certified by peer review) is the author/funder, who has granted bioRxiv a license to display the preprint in perpetuity. It is made available under aCC-BY-ND 4.0 International license.

local distribution of different neuropil components around a typical dendrite or an axon in neuropil. In the remainder of this article, we will also refer to such radial distribution functions in the case of neuropil specifically as the *neuropil structure functions*. In the case of structured neuropil organizations, we expect the correlations in the positions of neural processes in such neuropil to result in distinctive peaks and patterns in the structure functions.

We measure the radial distribution functions in hippocampal CA1 neuropil directly using the above electron microscopy reconstructions data (see Materials and Methods), Figure 2B. We observe that the measured structure functions are essentially flat at distances above 0.5 μm. A linear regression at the distance range of 0.5-2 μm gives the coefficient of regression for dendritic structure functions R=0.019±0.030 μm^{-1} with residual mean-square-error (MSE) MSE=0.0043±0.0022 μm^{-1} and for axonal structure functions R=-0.014±0.032 μm^{-1} and MSE=0.0035±0.0015 μm^{-1}. Therefore, this indicates that no significant correlations exist in the spatial organization of neural processes in hippocampal neuropil at the scales of one to several microns.

Measured structure functions exhibit a prominent peak-like feature at the distances of 0-0.5 μm, indicating correlations in the positions of neural processes at these distances. The origin of this peak can be traced to the effects of physical contact interaction of neural processes densely packed in neuropil. That is, if at large distances away from a reference process the neural processes can mix uniformly and disorderly, near the surface of that process the presence of its boundary itself causes adjacent neural processes to re-align along that boundary, resulting in correlations being induced in the positions of nearby processes, Figure 2C.

This effect can be understood quantitatively using a simple random mixing model of neuropil, see Materials and Methods. Such model reproduces well the features of observed neuropil structure functions. In particular, this model prescribes that near the surface of the reference object the ratio of the axonal and dendritic structure functions should equal the ratio of axonal and dendritic surface areas in neuropil. This ratio can be calculated from (Mishchenko et al., 2010) as 6:1, in good agreement with the structure functions in Figure 2. Furthermore, the random mixing model prescribes that at large distances the ratio of axonal and dendritic structure functions should equal the ratio of the volume densities of axonal and dendritic processes in the sample, which can be calculated as 2:1 (Mishchenko et al., 2010), again in good agreement with Figure 2. The transition between these two regimes occurs exponentially on the length scale of $l \approx 500$ nm, as defined primarily by the average dendritic diameter, also in agreement with Figure 2.

bioRxiv preprint doi: https://doi.org/10.1101/003863; this version posted April 8, 2014. The copyright holder for this preprint (which was not certified by peer review) is the author/funder, who has granted bioRxiv a license to display the preprint in perpetuity. It is made available under aCC-BY-ND 4.0 International license.

Finally, such model structure functions are the same around axonal and dendritic references, again in good agreement with the measurements.

We arrive at the conclusion, therefore, that the organization of hippocampal CA1 neuropil at the scales of one to several microns, as signified by measured neuropil structure functions, can be well understood using the model of locally disordered space-filling mixture of axonal and dendritic processes.

2. Orientational organization of hippocampal CA1 neuropil at micron scales

Even though the micron-scale organization of neural processes in neuropil may not exhibit any local ordering, it can still exhibit a global order such as directional alignment. In fact, it is well known from past anatomical studies that axonal and dendritic processes in hippocampus are organized in approximately perpendicular structures (Amaral and Witter, 1989; Cajal, 1909; Schaeffer, 1892; Westrum and Blackstad, 1962). Here, we measure the distribution of the headings of dendritic and axonal processes at micron scales, using electron microscopy reconstructions of the samples of hippocampal neuropil. We find that the approximately perpendicular organization of dendrites and axons is observed also at that very small scale, Figure 3. We observe that dendrites tend to run collinearly in the direction orthogonal to the plane of the CA1 cell-body layer and axons tend to orient themselves within that plane. The axonal component is found to possess a two-component structure with approximately half of the axons traveling in a collinear structure with single heading and the rest traversing the samples diffusely in all directions within the plane of the CA1 cell-body layer.

2. Micron-scale organization of glia and dendritic spines in hippocampal CA1 neuropil

The random mixing model prescribes that the distribution of neuropil components around a reference neural process should not be affected by the type of that process, either a dendrite or an axon. This property, in particular, is satisfied well by the micron-scale distributions of axonal and dendritic components. For the distribution of dendritic spines and glia, however, we observe deviations from that rule, revealed upon closer examination of the respective structure functions. In particular, the radial distribution of dendritic spines is observed to be significantly higher at the proximity of axonal rather than dendritic processes, and for glia we observe affinity towards dendrites as opposed to axons. Specifically, in the case of glia the mean relative density of glia near dendritic processes is measured to be 0.17 ± 0.01, while that near axonal surfaces is measured as 0.12 ± 0.01 (detailed data not shown). The relative densities of glia near dendritic and axonal processes, therefore, are different at p-value <0.001. One can note that for dendritic spines the preferential affinity towards axons may be natural, given that spines have to protrude away from dendrites and towards axons to establish synaptic contacts.

bioRxiv preprint doi: https://doi.org/10.1101/003863; this version posted April 8, 2014. The copyright holder for this preprint (which was not certified by peer review) is the author/funder, who has granted bioRxiv a license to display the preprint in perpetuity. It is made available under aCC-BY-ND 4.0 International license.

However, we are not aware of any known neurobiological mechanism that could account for the observed excess of glia near dendrites.

3. Distributions of local sizes of neural processes in hippocampal CA1 neuropil

The distribution of sizes of neural processes in neuropil has been a subject of significant interest in neurobiology (Braitenberg and Schuz, 1998; Mishchenko et al., 2010; Shepherd and Harris, 1998; Sorra and Harris, 2000). In particular, a comprehensive measurement of average neural processes' sizes had been performed in (Mishchenko et al., 2010). Here, we extend these measurements by characterizing the distribution of local neural processes' cross-section sizes, such as measured along a neural process' lengths. The sizes of axonal and dendritic processes are known to vary significantly over the space of just a few microns (Braitenberg and Schuz, 1998), and such local size distributions may be important for the understanding of the local organization of neuropil. The local size distributions that we measure are shown in Figure 4. We observe that such distributions are essentially exponential for all neuropil components. For spines, the exponential shape of size distribution had been known in the past, and an explanation had been offered based on information-theoretic arguments (Varshney et al., 2006). Here, we observe that exponential shape is characteristic of the local size distributions in all neuropil components, and a more generic reason may be appropriate. A particularly simple explanation can be offered based on the properties of exponential distributions as maximum entropy distributions (Jaynes, 2003), implying that the observed size distributions may be emerging in neuropil stochastically as the result of the competition of neural processes for limited volume resource (Chklovskii et al., 2002).

5. The relationship between local synaptic connectivity and micron-scale organization of neuropil

The nature of the relationship between local neuropil's organization and synaptic connectivity is important for neurobiology, since such organization has the potential to affect significantly the formation of synaptic connectivity on microscopic scales. The micron-scale organization and composition of neuropil, therefore, can play important role in development of synaptic connectivity as well as its disruptions. In order to examine this relationship, we study the variations in the spine density of different dendritic segments in the sample in relation to the structure of surrounding neuropil. We group all dendritic segments into three categories of high, medium, and low spine-density dendrites and compare the neuropil structure functions in such groups. The results of this measurement are presented in Figure5. We observe that the structure functions measured in such a way exhibit no significant variations, indicating lack of correlations between the local neuropil surrounding and the spine density of different dendritic segments, Figure

bioRxiv preprint doi: https://doi.org/10.1101/003863; this version posted April 8, 2014. The copyright holder for this preprint (which was not certified by peer review) is the author/funder, who has granted bioRxiv a license to display the preprint in perpetuity. It is made available under aCC-BY-ND 4.0 International license.

5B-D. A significant difference is observed in the distribution of the reference dendrites' own spines, Figure 5A, where the dendrites with higher spine density are also observed to exhibit a greater utilization of the nearby space for their spines. At the same time, the distribution of such spines is also observed to have the same shape in all cases, thus indicating that the dendrites place their spines in the same zone at about 400 nm away from the shaft regardless of the spine density. In the case of the spines of neaby dendrites, Figure 4B, we observe that that distribution is essentially flat (the coefficient of linear regression R=0.0090 μm^{-1} with MSE=0.0031 μm^{-1}), indicating that the spines of nearby dendrites are unaffected by the presence of the reference dendrite. That is, the spine zones of nearby dendrites overlap and interpenetrate in neuropil freely and without interactions.

DISCUSSION

While the ubiquity of different anatomical structures in the brain at macro and mesoscales is well known, the structural organization of the brain at the smallest, micron scales remains largely unknown. In this work, we aim to fill this gap by examining the structural organization of neural tissue using dense electron microscopy reconstructions of neuropil in hippocampal area CA1.

Dense reconstructions of neuropil in (Mishchenko, 2009; Mishchenko and Paninski, 2012; Rivera-Alba et al., 2011) offer unique insights into neuropil organization in the sense that they not only provide the reconstructions of a large number of dendritic and axonal processes at nanometer resolution, but also place these in the context of their immediate neuropil surrounding. To gain novel insights into the micron-scale structural organization of neural tissue here, we calculate the radial distribution functions for hippocampal area CA1 neuropil using such reconstructions. We analyze produced results statistically and using a modeling approach. Our analysis demonstrates that the micron-scale organization of neuropil is essentially consistent with disordered, random packing of axonal and dendritic processes. At very small distances below 500 nm correlations among neural processes are observed, attributed to the physical contact interactions of neural processes in the settings of dense space-filling packing in neuropil. We also present the measurements of local size distributions and orientational anisotropy of neural tissue at micron scale. Our observations paint a picture of micron-scale neuropil's organization as a randomized system of axonal and dendritic processes without significant interactions beyond direct physical contact and without significant small-scale features.

We observe deviations in the micron-scale distributions of dendritic spines and glia, whereas dendritic spines are observed to be preferentially located near axonal processes and glia is observed with higher frequency near dendritic processes. While for dendritic

bioRxiv preprint doi: https://doi.org/10.1101/003863; this version posted April 8, 2014. The copyright holder for this preprint (which was not certified by peer review) is the author/funder, who has granted bioRxiv a license to display the preprint in perpetuity. It is made available under aCC-BY-ND 4.0 International license.

spines the observed affinity can be expected given that spines protrude away from dendrites in order to contact axons and create synapses, there are no similar known mechanisms that could explain the observed excess of glia near dendrites. These observations, therefore, may indicate the presence of yet unknown neurobiological mechanisms affecting the development of glia in neuropil.

We finally examine the question of the interactions between local neuropil and synaptic connectivity. While it may be naturally expected that the local organization and composition of neuropil can affect strongly the small-scale synaptic connectivity in neural tissue, we do not observed that to be the case. Indeed, we observe that the local connectivity of different dendritic segments appears to vary completely independently of the features of the surrounding neuropil, implying that synaptic connectivity is largely unaffected by immediately surrounding neuropil.

It should be noted that our findings here had been produced using a limited sample of hippocampal CA1 neuropil and, therefore, may not apply in other circumstances. Nonetheless, as the past neuroanatomical literature indicates a substantial similarity in the organization of neural tissues in different cortical regions (Braitenberg and Schuz, 1998), we may believe that the observations here may be indicative of the organization of neuropil in mammalian cerebral cortex more generally.

ACKNOWLEDGEMENTS

The author acknowledges the financial support from Bilim Akademisi – The Science Academy, Turkey, under BAGEP program and the support from the BAP fund – the Fund for Scientific Research Projects, of Toros University, Mersin, Turkey.

REFERENCES

Adams, D.L., and Horton, J.C. (2003). A Precise Retinotopic Map of Primate Striate Cortex Generated from the Representation of Angioscotomas. J. Neurosci. *23*, 3771–3789.

Amaral, D.G., and Witter, M.P. (1989). The three-dimensional organization of the hippocampal formation: a review of anatomical data. Neuroscience *31*, 571–591.

Arbib, M.A., Erdi, P., and Szentagothai, J. (1997). Neural Organization: Structure, Function, and Dynamics (A Bradford Book).

bioRxiv preprint doi: https://doi.org/10.1101/003863; this version posted April 8, 2014. The copyright holder for this preprint (which was not certified by peer review) is the author/funder, who has granted bioRxiv a license to display the preprint in perpetuity. It is made available under aCC-BY-ND 4.0 International license.

Bonda, D.J., Bajić, V.P., Spremo-Potparevic, B., Casadesus, G., Zhu, X., Smith, M.A., and Lee, H.-G. (2010). Review: Cell cycle aberrations and neurodegeneration. Neuropathol. Appl. Neurobiol. *36*, 157–163.

Bono, M., and Villu Maricq, A. (2005). Neuronal substrates of complex behaviors in C. elegans. Annu. Rev. Neurosci. *28*, 451–501.

Bosking, W.H., Zhang, Y., Schofield, B., and Fitzpatrick, D. (1997). Orientation Selectivity and the Arrangement of Horizontal Connections in Tree Shrew Striate Cortex. J. Neurosci. *17*, 2112–2127.

Braitenberg, V., and Schuz, A. (1998). Cortex: statistics and geometry of neuronal connectivity. (Berlin: Springer).

Brambilla, P., Hardan, A., di Nemi, S.U., Perez, J., Soares, J.C., and Barale, F. (2003). Brain anatomy and development in autism: Review of structural MRI studies. Brain Res. Bull. *61*, 557–569.

Brodmann, K., and Garey, L.J. (2005). Brodmann's: Localisation in the Cerebral Cortex (Springer).

Cajal, R. (1909). Histologie du systeme nerveux de l'homme & des vertebres (Paris: Maloine).

Castellanos, F.X., Lee, P.P., Sharp, W., Jeffries, N.O., Greenstein, D.K., Clasen, L.S., Blumenthal, J.D., James, R.S., Ebens, C.L., Walter, J.M., et al. (2002). Developmental Trajectories of Brain Volume Abnormalities in Children and Adolescents With Attention-Deficit/Hyperactivity Disorder. J. Am. Med. Assoc. *288*, 1740–1748.

Chandler, D. (1987). Introduction to Modern Statistical Mechanics (New York: Oxford University Press).

Chicurel, M., and Harris, K.M. (1992). Three-dimensional analysis of the structure and composition of CA3 branched dendritic spines and their synaptic relationships with mossy fiber boutons in the rat hippocampus. J. Comput. Neurol. *325*, 169–182.

Chklovskii, D.B., Schikorski, T., and Stevens, C.F. (2002). Wiring optimization in cortical circuits. Neuron *34*, 341–347.

bioRxiv preprint doi: https://doi.org/10.1101/003863; this version posted April 8, 2014. The copyright holder for this preprint (which was not certified by peer review) is the author/funder, who has granted bioRxiv a license to display the preprint in perpetuity. It is made available under aCC-BY-ND 4.0 International license.

Damasio, H. (2005). Human Brain Anatomy in Computerized Images (Oxford university press).

Dickson, B.J. (2002). Molecular mechanisms of axon guidance. Science (80-.). *298*, 1959–1964.

Erwin, E., Obermayer, K., and Schulten, K. (1995). Models of Orientation and Ocular Dominance Columns in the Visual Cortex: A Critical Comparison. Neural Comput. *7*, 425–468.

Ferster, D., and Miller, K.D. (2000). Neural Mechanisms of Orientation Selectivity in the Visual Cortex. Annu. Rev. Neurosci. *23*, 441–471.

Fiala, J.C.C., and Harris, K.M.M. (2001). Extending unbiased stereology of brain ultrastructure to three-dimensional volumes. J. Am. Med. Informatics Assoc. *8*, 1–16.

Fiala, J.C., Kirov, S.A., Feinberq, M.D., Petrak, L.J., George, P., Goddard, C.A., and Harris, K.M. (2003). Timing of neuronal and glial ultrastructure disruption during brain slice preparation and recovery in vitro. J. Comput. Neurol. *465*, 90–103.

Freeman, R.D.D. (2003). Cortical columns: a multi-parameter examination. Cereb. Cortex *13*, 70.

Garrard, P., Patterson, K., Watson, P.C., and Hodges, J.R. (1998). Category specific semantic loss in dementia of Alzheimer's type. Functional-anatomical correlations from cross-sectional analyses. Brain *121*, 633–646.

Geschwind, N. (1975). The Apraxias: Neural Mechanisms of Disorders of Learned Movement. Am. Sci. *63*, 188–195.

Good, C.D., Scahill, R.I., Fox, N.C., Ashburner, J., Friston, K.J., Chan, D., Crum, W.R., Rossor, M.N., and Frackowiak, R.S.J. (2002). Automatic Differentiation of Anatomical Patterns in the Human Brain: Validation with Studies of Degenerative Dementias. Neuroimage *17*, 29–46.

Hamos, J.E., DeGennaro, L.J., and Drachman, D.A. (1989). Synaptic loss in Alzheimer's disease and other dementias. Neurology *39*, 355.

bioRxiv preprint doi: https://doi.org/10.1101/003863; this version posted April 8, 2014. The copyright holder for this preprint (which was not certified by peer review) is the author/funder, who has granted bioRxiv a license to display the preprint in perpetuity. It is made available under aCC-BY-ND 4.0 International license.

Harris, K.M., and Stevens, J.K. (1989). Dendritic spines of CA 1 pyramidal cells in the rat hippocampus: serial electron microscopy with reference to their biophysical characteristics. J. Neurosci. *9*, 2982–2997.

Hatton, G.I. (1990). Emerging concepts of structure-function dynamics in adult brain: the hypothalamo-neurohypophysial system. Prog. Neurobiol. *34*, 437–504.

Jaynes, E.T. (2003). Probability Theory: The Logic of Science. (New York: Cambridge University Press).

Kandel, E., Schwartz, J., and Jessell, T. (2000). Principles of Neural Science (McGraw-Hill Medical).

Keil, W., Schmidt, K.F., Löwel, S., and Kaschube, M. (2010). Reorganization of columnar architecture in the growing visual cortex. Proc. Natl. Acad. Sci. *107*, 12293.

McLaughlin, T., and O'Leary, D.M. (2005). Molecular gradients and development of retinotopic maps. Annu. Rev. Neurosci. *28*, 327–355.

McQuarrie, D.A. (2000). Statistical Mechanics (University Science Books).

Miller, K.D., Keller, J.B., and Stryker, M.P. (1989). Ocular dominance column development: analysis and simulation. Science (80-.). *245*, 605–615.

Mishchenko, Y. (2009). Automation of 3D reconstruction of neural tissue from large volume of conventional serial section transmission electron micrographs. J. Neurosci. Methods *176*, 276–289.

Mishchenko, Y. (2013). A function for fast computation of large discrete Euclidean distance transforms in three or more dimensions in Matlab. Signal, Image Video Process.

Mishchenko, Y., and Paninski, L. (2012). Efficient methods for sampling spike trains in networks of coupled neurons. Ann. Appl. Stat. *5*, 1893–1919.

Mishchenko, Y., Hu, T., Spacek, J., Mendenhall, J., Harris, K.M., and Chklovskii, D.B. (2010). Ultrastructural analysis of hippocampal neuropil from the connectomics perspective. Neuron *67*, 1009–1020.

bioRxiv preprint doi: https://doi.org/10.1101/003863; this version posted April 8, 2014. The copyright holder for this preprint (which was not certified by peer review) is the author/funder, who has granted bioRxiv a license to display the preprint in perpetuity. It is made available under aCC-BY-ND 4.0 International license.

Montero, V.M., Guillery, R.W., and Woolsey, C.N. (1977). Retinotopic organization within the thalamic reticular nucleus demonstrated by a double label autoradiographic technique. Brain Res. *138*, 407–421.

Nolte, J. (2002). The Human Brain: An Introduction to Its Functional Anatomy (Mosby).

Ohki, K., Chung, S., Chung, Y.H., Kara, P., and Reid, R.C. (2005). Functional imaging with cellular resolution reveals precise micro-architecture in visual cortex. Neuron *433*, 597–603.

Parrish, J.Z., Emoto, K., Kim, M.D., and Jan, Y.N. (2007). Mechanisms that regulate establishment, maintenance, and remodeling of dendritic fields. Annu. Rev. Neurosci. *30*, 399–423.

Raff, M.C., Whitmore, A. V., and Finn, J.T. (2002). Axonal Self-Destruction and Neurodegeneration. Science (80-.). *296*, 868–871.

Rivera-Alba, M., Vitaladevuni, S.N., Mishchenko, Y., Lu, Z., Takemura, S.-Y., Scheffer, L., Meinertzhagen, I.A., Chklovskii, D., and de Polavieja, G.G. (2011). Wiring economy and volume exclusion determine neuronal placement in the Drosophila brain. Curr. Biol. *21*, 2000–2005.

Sandler, S.I. (2010). An Introduction to Applied Statistical Thermodynamics (John Wiley & Sons).

Schaeffer, K. (1892). Beitrag zur Histologie der Ammonshornformation. Arch Mikrosc Anat *39*, 611–632.

Scheff, S.W., Price, D.A., Schmitt, F.A., and Mufson, E.J. (2006). Hippocampal synaptic loss in early Alzheimer's disease and mild cognitive impairment. Neurobiol. Aging *27*, 1372–1384.

Shepherd, G.M., and Harris, K.M. (1998). Three-dimensional structure and composition of CA3-->CA1 axons in rat hippocampal slices: implications for presynaptic connectivity and compartmentalization. J. Neurosci. *18*, 8300–8310.

Sorra, K.E., and Harris, K.M. (2000). Overview on the structure, composition, function, development, and plasticity of hippocampal dendritic spines. Hippocampus *10*, 501–511.

bioRxiv preprint doi: https://doi.org/10.1101/003863; this version posted April 8, 2014. The copyright holder for this preprint (which was not certified by peer review) is the author/funder, who has granted bioRxiv a license to display the preprint in perpetuity. It is made available under aCC-BY-ND 4.0 International license.

Sporns, O., Chialvo, D.R., Kaiser, M., and Hilgetag, C.C. (2004). Organization, development and function of complex brain networks. Trends Cogn. Sci. *8*, 418–426.

Sporns, O., Tononi, G., and Kötter, R. (2005). The human connectome: a structural description of the human brain. PLoS Comput. Biol. *1*, e42.

Tear, G. (1999). Neuronal guidance: a genetic perspective. Trends Neurosci. *15*, 113–118.

Terry, R.D. (2000). Cell Death or Synaptic Loss in Alzheimer Disease. J. Neuropathol. Exp. Neurol. *59*, 1118–1119.

Uhlhaas, P.J., and Singer, W. (2006). Neural Synchrony in Brain Disorders: Relevance for Cognitive Dysfunctions and Pathophysiology. Neuron *52*, 155–168.

Varshney, L.R., Sjöström, P.J., and Chklovskii, D.B. (2006). Optimal information storage in noisy synapses under resource constraints. Neuron *52*, 409–423.

Westrum, L.E., and Blackstad, T.W. (1962). An electron microscopic study of the stratum radiatum of the rat hippocampus (regio superior, CA 1) with particular emphasis on synaptology. J. Comput. Neurol. *119*, 281–309.

Wolf, L., Goldberg, C., Manor, N., Sharan, R., and Ruppin, E. (2011). Gene expression in the rodent brain is associated with its regional connectivity. PLoS Comput. Biol. *7*, e1002040.

Wong, R.O.L. (1999). Retinal waves and visual system development. Annu. Rev. Neurosci. *22*, 29–47.

bioRxiv preprint doi: https://doi.org/10.1101/003863; this version posted April 8, 2014. The copyright holder for this preprint (which was not certified by peer review) is the author/funder, who has granted bioRxiv a license to display the preprint in perpetuity. It is made available under aCC-BY-ND 4.0 International license.

FIGURE CAPTIONS

Figure 1: Dense ssTEM reconstructions of hippocampal CA1 neural tissue reveal complex structural organization of neuropil at micron scales. (A) An example of the 3D dense ssTEM reconstruction "Volume 1" in (Mishchenko et al., 2010); spanning $9.1 \times 9.0 \times 4.1$ μm^3 and 800 different neural processes (left), and an example of the 3D dense ssTEM reconstruction "Volume 4" in (Mishchenko, 2009), spanning $6.0 \times 4.3 \times 5.1$ μm^3 and 350 neural processes (right). Different colors represent neural processes of different types: green for axons, yellow for dendrites, magenta for spines, and blue for glia. Gray represents unclassified objects. (B) Examples of 2D micrographs from "Volume 1" (left) and "Volume 4" (right).

Figure 2: Radial distribution functions for micron-scale organization of hippocampal CA1 neuropil. (A) Radial distribution functions offer a powerful tool for accurate characterization of the distributions of different neuropil components in the immediate surroundings of typical dendrites and axons in neuropil. Here, the calculation of a radial distribution function is exemplified using a series of radial shells constructed at different distances away from the surface of one reference dendrite (left) and one reference axon (right). Radial distribution functions are defined as the average density of neural processes of different kind at different distances away from such reference axon or dendrite. (B) The radial distribution functions measured for axonal and dendritic processes in the sample volumes 1, 3 and 4. The measured radial distributions show flat behavior, indicating that the organization of neuropil at micron scales does not exhibit significant spatial correlations. The error bars represent the variation of radial distribution functions measured around different axons and dendrites in the samples.

Figure 3: The micron-scale directional organization of hippocampal CA1 neuropil. (A) The distribution of dendritic headings measured in different samples shown in azimuthal projection centered on the dominant orientation of dendritic processes, in count per steradian of solid angle. (B) The distribution of measured axonal headings shown in the same projection. The measurements of the directional organization of hippocampal CA1 neuropil reveal approximately perpendicular organization of dendrites and axons in hippocampal CA1 neuropil at micron scales. The dendrites are found to run collinearly in the direction perpendicular to the plain of the CA1 cell-body layer, while the axons are found to run predominantly within that plane. Additionally, axons exhibit two distinctive directional components: a collinear component and a diffuse component, containing approximately 50% of axons each.

Figure 4: The distribution of local cross-section sizes for axonal and dendritic processes. (A) The distribution of local sizes of axonal cross-sections in sample volumes

bioRxiv preprint doi: https://doi.org/10.1101/003863; this version posted April 8, 2014. The copyright holder for this preprint (which was not certified by peer review) is the author/funder, who has granted bioRxiv a license to display the preprint in perpetuity. It is made available under aCC-BY-ND 4.0 International license.

1, 3 and 4, normalized to the average axonal cross-section in each volume. (B) The distribution of local sizes of dendritic cross-sections in sample volumes 1, 3 and 4, normalized to the average dendritic cross-section in each volume. All distributions are well described by similar maximal entropy exponential distributions, suggesting a common mechanism for their origin.

Figure 5: The organization of neuropil around dendritic segments with different spine densities. (A) The radial distributions of reference dendrites' own spines reveal higher utilization of proximal neuropil for placing spines by higher spine-density dendrites. (B-D) The other radial distributions exhibit no significant differences in relation to the reference dendrites' spine-density. Shown here are (B) the radial distribution of the spines of other dendrites, (C) the radial distribution of axons, and (D) the radial distribution of glia, graded by the spine density of the reference dendrite. Here, the low spine-density group corresponded to the lowest 50% of spine densities, next 25% comprised the medium spine-density group, and the highest 25% comprised the high-density group. The legend shown is for all graphs. The error bars are the standard errors of the mean.

bioRxiv preprint doi: https://doi.org/10.1101/003863; this version posted April 8, 2014. The copyright holder for this preprint (which was not certified by peer review) is the author/funder, who has granted bioRxiv a license to display the preprint in perpetuity. It is made available under aCC-BY-ND 4.0 International license.

SUPPLEMENT: RADIAL DISTRIBUTION FUNCTIONS

Radial distribution functions, also known as pairwise correlation functions, are defined in statistical physics as the average density of particles of given sort at different distances away from a given reference particle. Radial distribution functions characterize spatial correlations present in a material and provide a powerful tool for systematic quantification of the small-scale organization of complex materials and systems. Respectively, in material sciences the radial distribution functions have been commonly used to characterize the organization of complex materials such as alloys, solutions, colloids, etc. Radial distributions in ordered materials, due to strong correlations in the positions of their structural elements, exhibit distinctive peaks and other features, while in disordered materials absence of any strong correlations results in the radial distribution functions without any significant features.

In Supplementary Figure 1, we provide an example of simulated radial distribution functions for different possible arrangements of neural processes in neuropil tissue, ranging from completely disordered to completely ordered. Panel (A) shows an example of such an arrangement that is completely ordered, that is, where all neural processes move in the same direction and are perfectly aligned spatially (left). The radial distribution function in such a model arrangement is shown in the right. As can be seen there, the respective radial distribution function shows strong peaks representative of the strong correlations present in the positions of neural processes in this arrangement. Panel (B) shows a similar arrangement where neural processes are partially disordered, that is, where the positions of different processes are less well coordinated and their headings slightly vary. In such a partially ordered arrangement the radial distribution still exhibits peak-like features, but the peaks become much smoother and less pronounced due to destruction of the correlations. Finally, in panel (C) we give an example of a model arrangement that is completely disordered, that is, where the headings of neural processes are completely random as are their positions. The radial distribution function, respectively, is obtained as completely flat and without any features.

bioRxiv preprint doi: https://doi.org/10.1101/003863; this version posted April 8, 2014. The copyright holder for this preprint (which was not certified by peer review) is the author/funder, who has granted bioRxiv a license to display the preprint in perpetuity. It is made available under aCC-BY-ND 4.0 International license.

Mishchenko Fig. 1

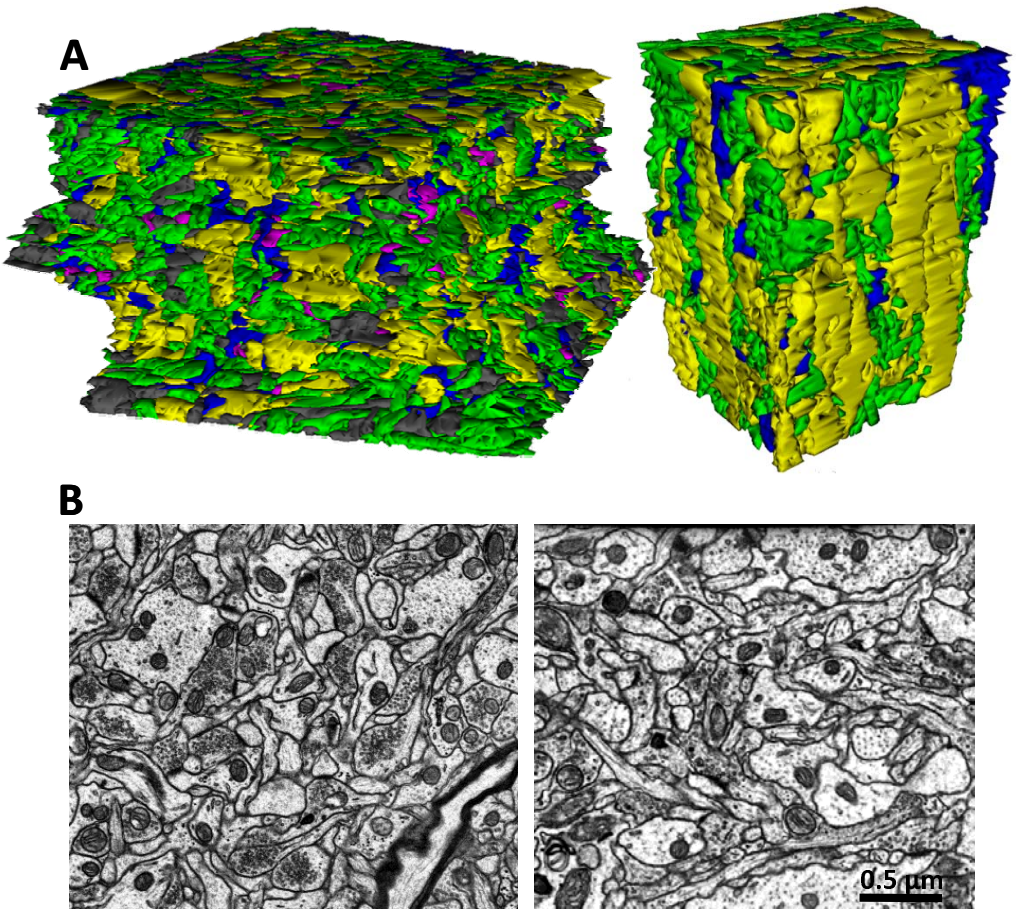

bioRxiv preprint doi: https://doi.org/10.1101/003863; this version posted April 8, 2014. The copyright holder for this preprint (which was not certified by peer review) is the author/funder, who has granted bioRxiv a license to display the preprint in perpetuity. It is made available under aCC-BY-ND 4.0 International license.

Mishchenko Fig. 2

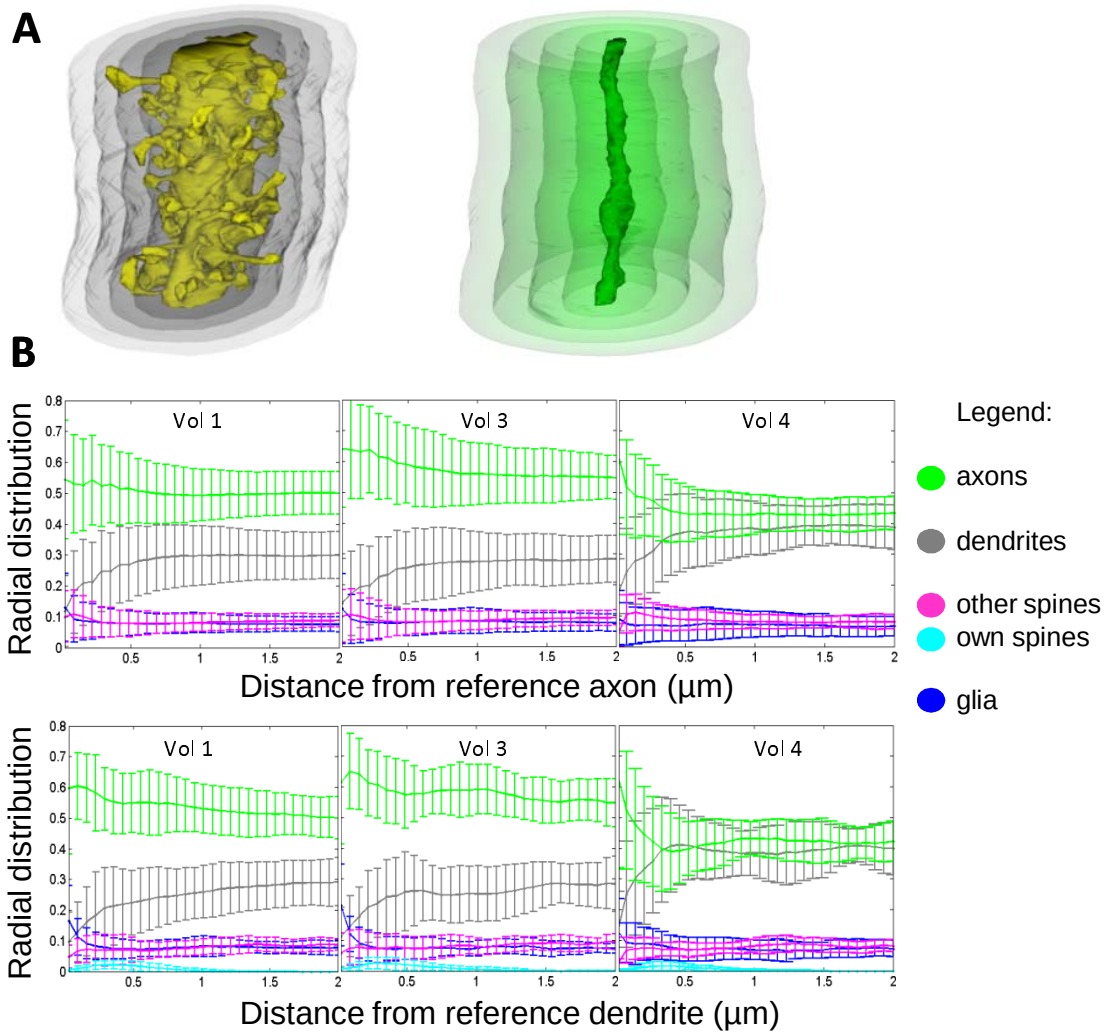

bioRxiv preprint doi: https://doi.org/10.1101/003863; this version posted April 8, 2014. The copyright holder for this preprint (which was not certified by peer review) is the author/funder, who has granted bioRxiv a license to display the preprint in perpetuity. It is made available under aCC-BY-ND 4.0 International license.

Mishchenko Fig. 3

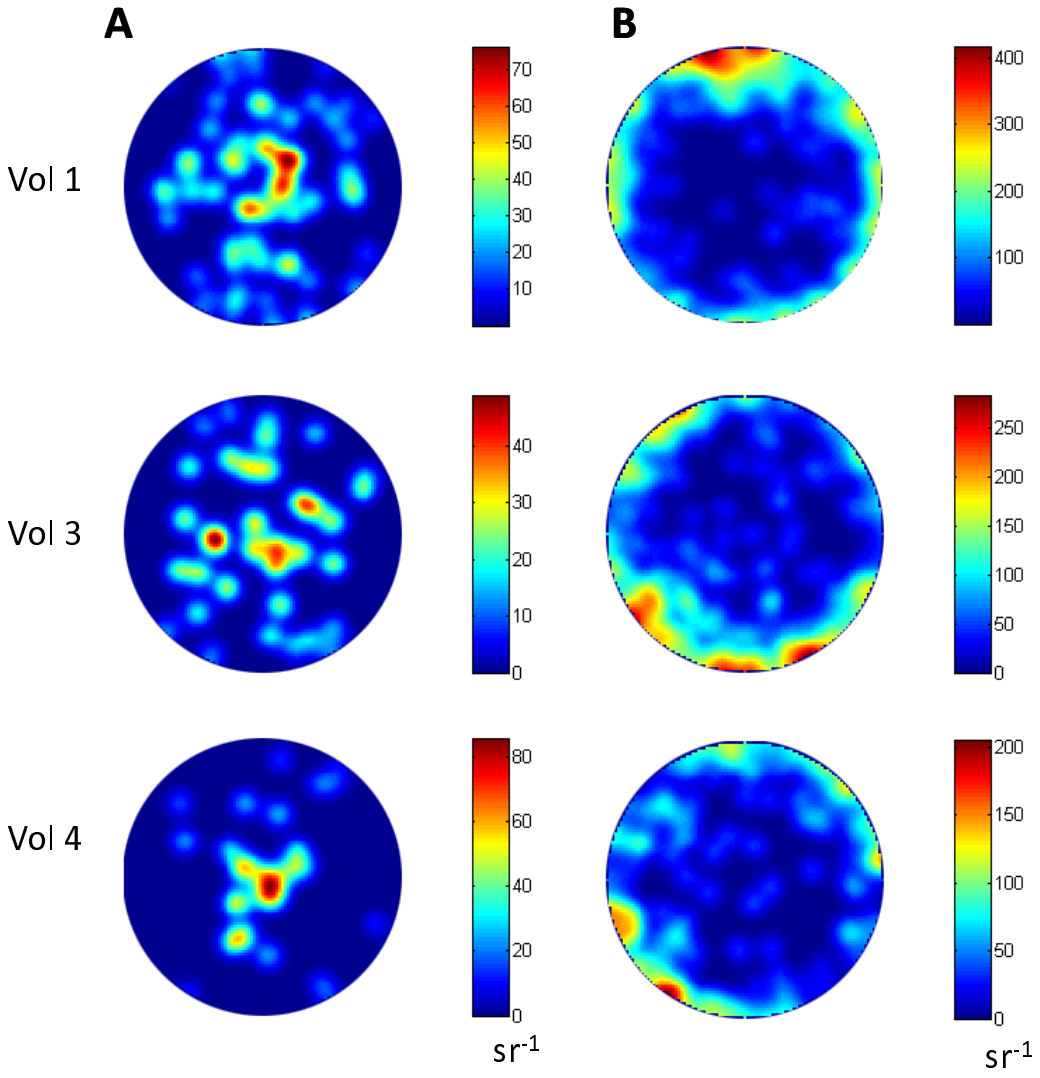

bioRxiv preprint doi: https://doi.org/10.1101/003863; this version posted April 8, 2014. The copyright holder for this preprint (which was not certified by peer review) is the author/funder, who has granted bioRxiv a license to display the preprint in perpetuity. It is made available under aCC-BY-ND 4.0 International license.

Mishchenko Fig. 4

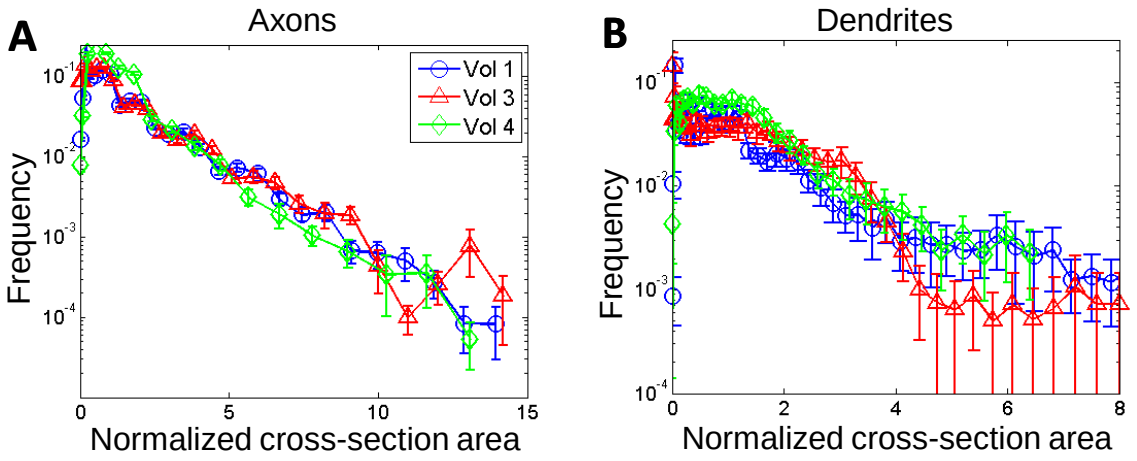

bioRxiv preprint doi: https://doi.org/10.1101/003863; this version posted April 8, 2014. The copyright holder for this preprint (which was not certified by peer review) is the author/funder, who has granted bioRxiv a license to display the preprint in perpetuity. It is made available under aCC-BY-ND 4.0 International license.

Mishchenko Fig. 5

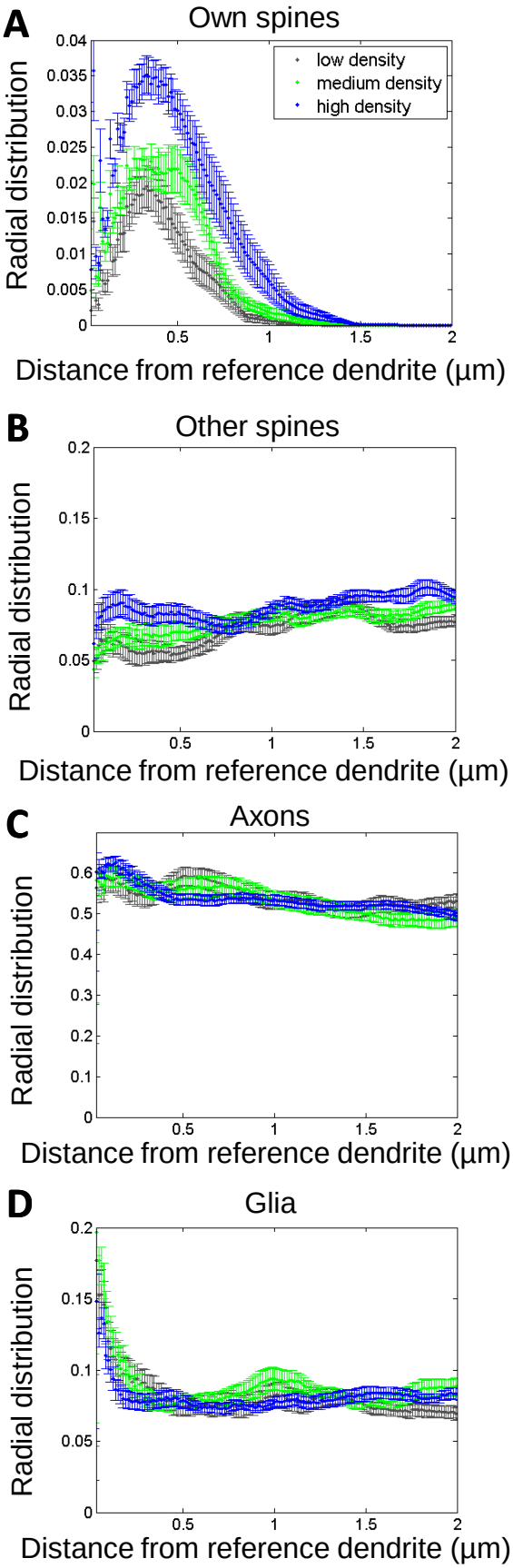

bioRxiv preprint doi: https://doi.org/10.1101/003863; this version posted April 8, 2014. The copyright holder for this preprint (which was not certified by peer review) is the author/funder, who has granted bioRxiv a license to display the preprint in perpetuity. It is made available under aCC-BY-ND 4.0 International license.

Suppl. Fig. 1
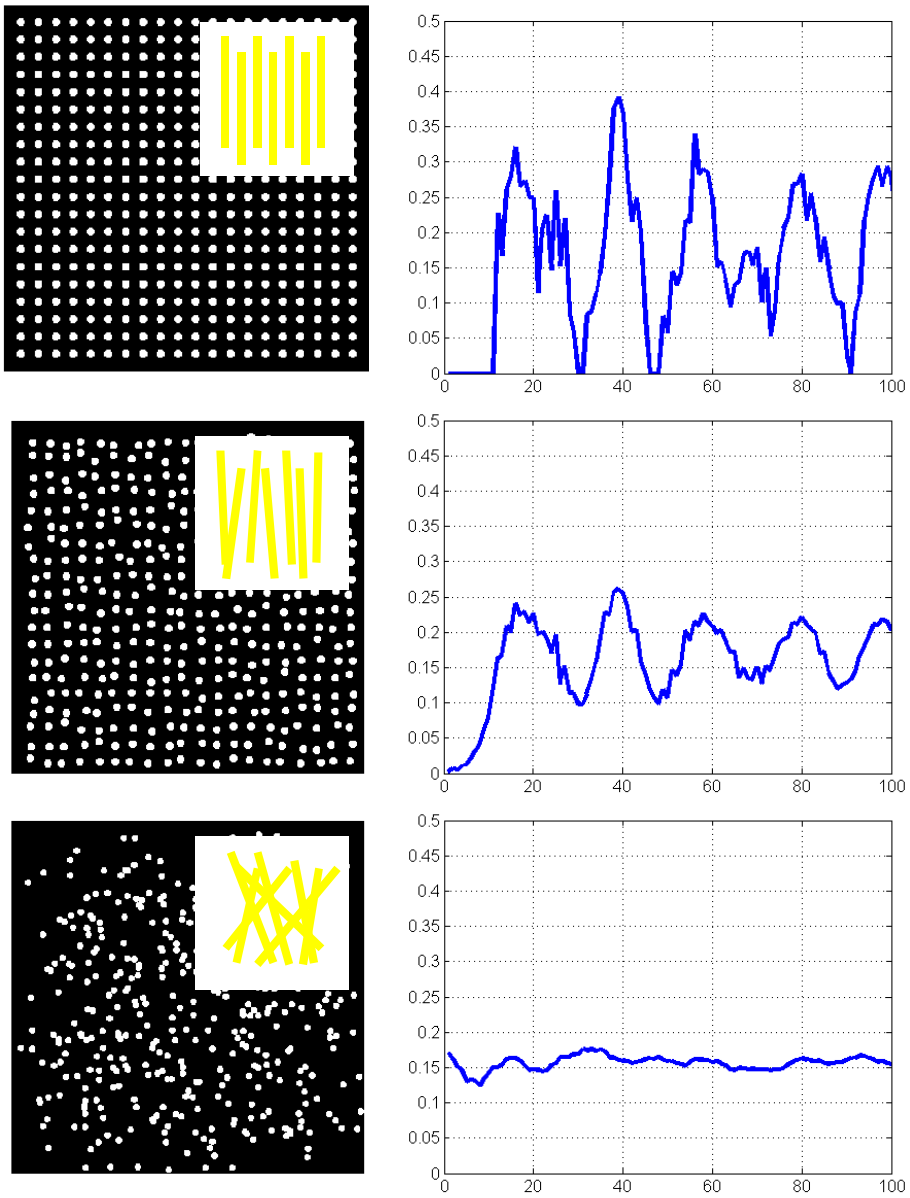
A